Report On Ageing Studies On LAPPD#153

Jinky Agarwala, On behalf of INFN, Trieste

September 2024

Contents

Ageing studies on LAPPD #153

1.1 Introduction

Ageing effects had been measured on the LAPPD #153 in the laboratory of INFN, Trieste. The LAPPD was placed in a dedicated light-tight dark-box. A moving-arm system, controlled by Zaber software, had also been installed inside the dark-box. Two fibres from two light sources, a pulsed laser and a continuous LED both of wavelength 405 nm, were mounted on the horizontal arm of the moving system as shown in Figure 1.1. The ageing tests were performed on four lateral sensor pads on a custom-designed PCB. A region of the LAPPD window aligned with sensor pads #1-2-3-4 was exposed to substantial light integrals sent by the continuous LED, whereas another region aligned with sensor pads #5-6-7-8 that were used as the reference pads for comparison, was illuminated by the pulsed laser. The mapping of the sensor pads is shown in Figure 1.2. The LAPPD window was well protected by a black screen while substantial illumination was introduced to the region through a hole of diameter 2.4 cm on the black screen. Hence, the illuminated area was $\sim 4.53\ cm^2$.

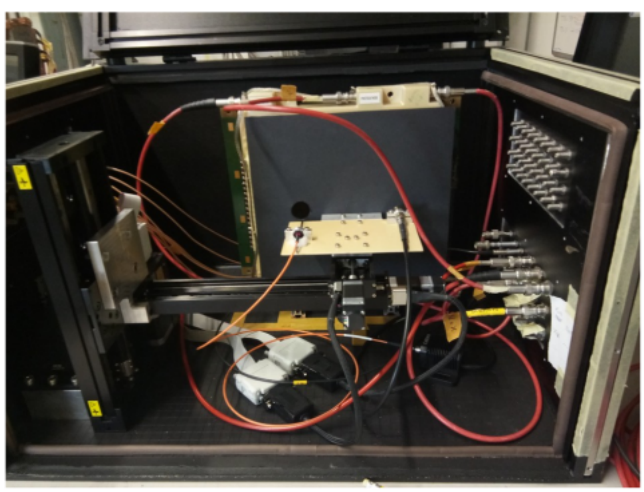

Figure 1.1: The LAPPD #153 along with a moving-arm system has been installed inside a light-tight dark-box. Fibres from a continuous LED and a pulsed laser and a black screen with two holes were mounted on the horizontal arm of the moving system.

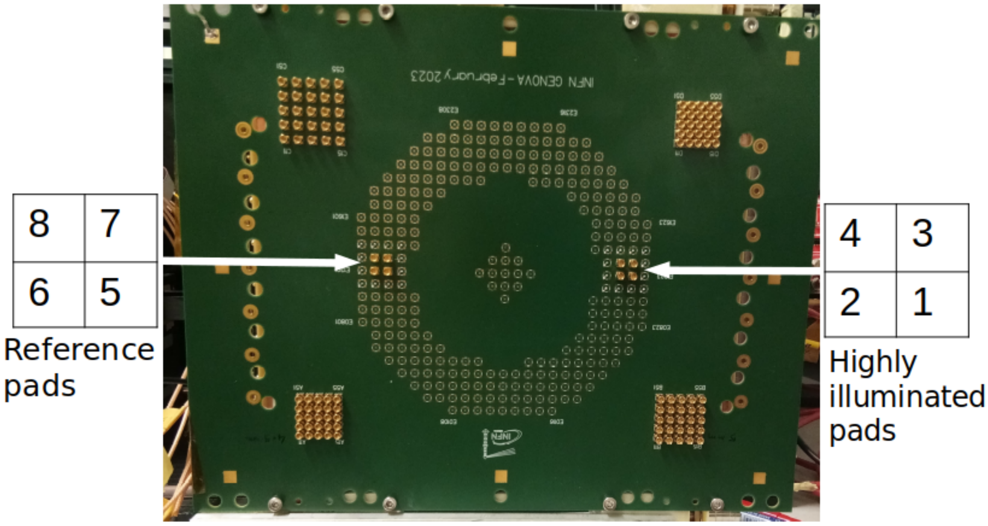

Figure 1.2: Mapping of the eight lateral pads, with SMA connectors mounted, is shown. The view of this mapping is opposite to the photon view, i.e., from the PCB to the LAPPD window. Two regions of four pads are well separated from each other.

Negative voltages with respect to the anode were distributed and controlled independently at the five electrodes, namely, the Photo-Cathode (PC), the Entry of the Entry MCP (NoN), the Exit of the Entry MCP (XoN), the Entry of the Exit MCP (NoX) and the Exit of the Exit MCP (XoX). The nominal biasing voltages applied at the XoX, NoX, XoN and NoN were - 200 V, - 1025 V, - 1225 V, and - 2050 V, respectively, while the PC was kept at the maximum negative potential of - 2080 V. Accordingly, the differential High Voltage (HV) potential applied at XoX-NoX-XoN-NoN-PC were 200-825-200-825-30 V, respectively. The gain of the LAPPD at this voltage configuration, provided by Incom datasheet, is $\sim 1.2 \times 10^6$. The intensity of the pulsed laser was selected to be 1.7 and this value was untouched during all the measurements. For measuring the integrated charge at the PC and Anode, several custom-designed picoammeters[1] of resolution 1 pA and a picoammeter from Keithley, Tektronix (model 6485) of resolution 10 fA were used, respectively. The picoammeters were calibrated using known resistors of ~ 20 GΩ and ~ 10 MΩ and a low voltage power supply. They showed good linearity as can be seen in Figures 1.3-left and 1.3-right. For the custom-made picoammeters, the evolution of current in time for a fixed voltage and a fixed resistor was measured. A fluctuation in the current had been observed, in particular, at the beginning of the measurement. This fluctuation is shown, Figure 1.4, for one of the devices. So, in order to have lower fluctuation, we turn On the device well before a measurement was started. The electronic circuit for the experimental set-up is illustrated in Figure 1.5.

The strategy of the ageing studies has been the following:

1. Comparison of the effective Quantum Efficiency (QE), the signal amplitude and the Dark Count Rate (DCR) before and after exposing the LAPPD window to substantial illumination.

2. Monitoring the currents both at the PC and Anode in order to measure the

[1] https://pos.sissa.it/322/068/pdf

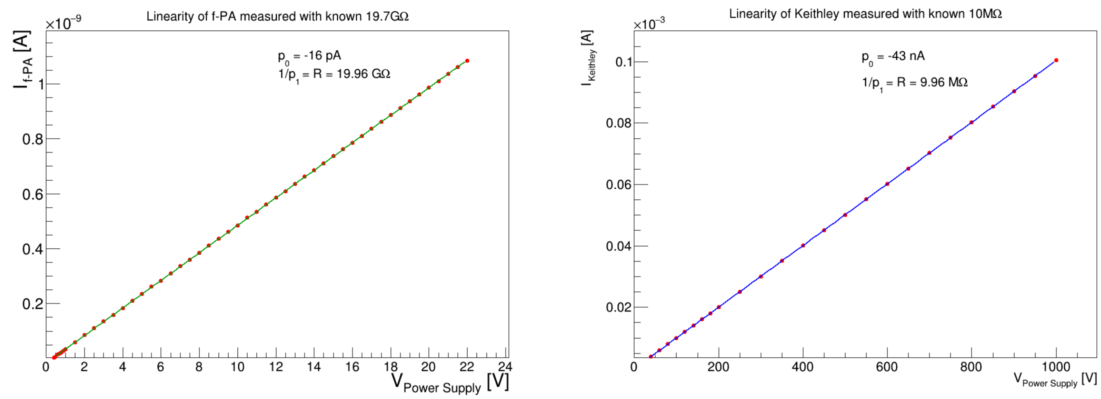

Figure 1.3: The custom-made picoammeter (left) and the Keithley-6485 (right) show good linearity measured using a $\sim$ 20 GΩ and $\sim$ 10 MΩ resistors, respectively.

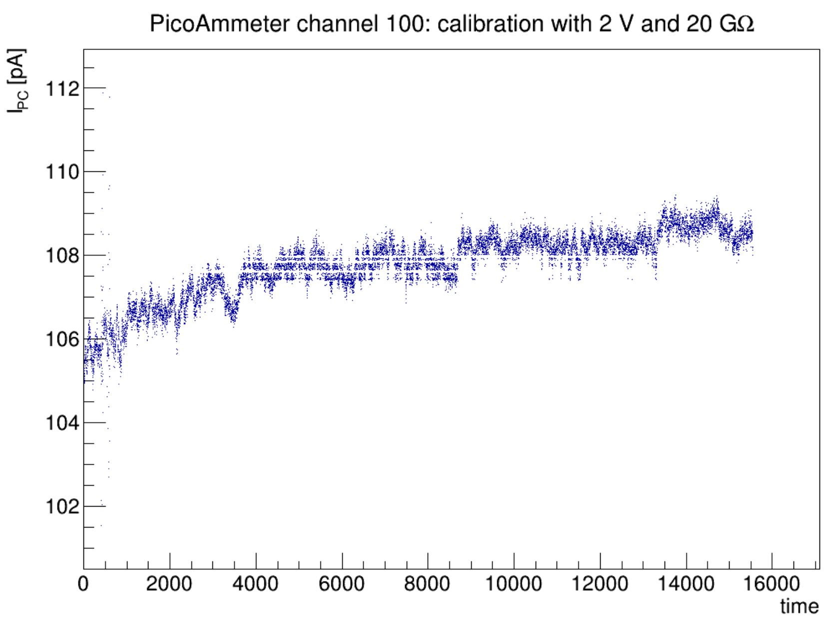

Figure 1.4: The current provided by a custom-made picoammeter, for a fixed voltage of 2 V and fixed resistance of 20 GΩ, shows a fluctuation in time.

amount of total integrated charge after illumination at these electrodes.

A report dedicated to the detail of these measurements has been presented in the following sections.

1.2 Position determination of sensor pads

In order to determine the coarse position of the eight pads with respect to the position of the fibre tip from the light sources, rate scans were performed in a step of 1 mm along both horizontal and vertical directions. The pulsed laser at an intensity 1.7 and an internal trigger rate of 2.5 MHz (80 MHz/32) was used for this exercise. An inverting amplifier (of Gain = 10) was installed after the pads in the readout chain. Number of

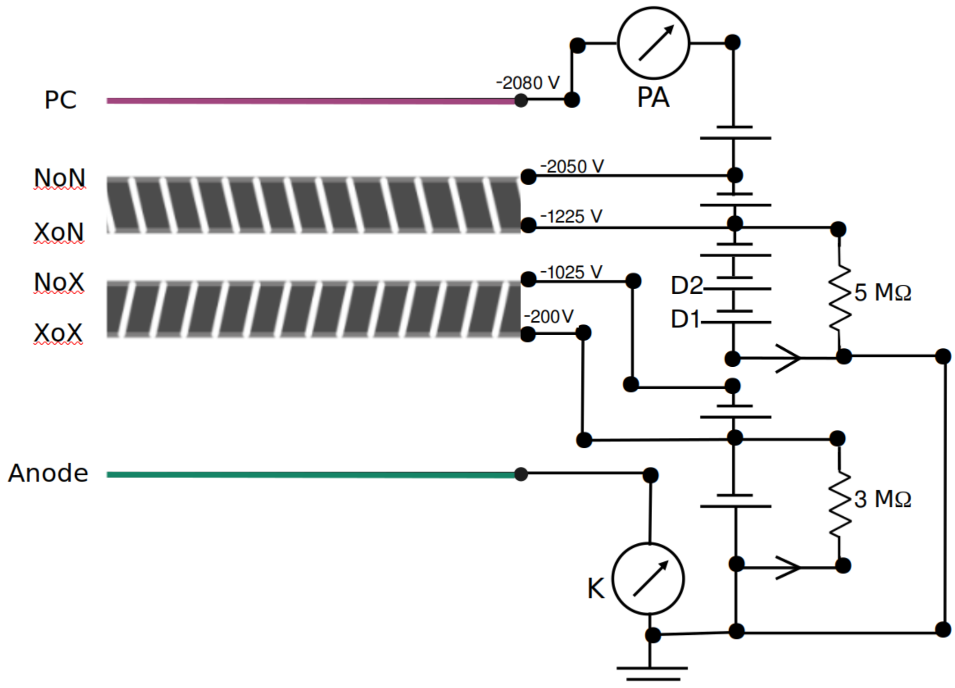

Figure 1.5: The electronic circuit for the experimental set-up of the LAPPD ageing studies is illustrated. The nominal biasing voltages are depicted. Seven channels from the CAEN DT1415 HV power supply are used in "Daisy chain" to power the five electrodes. Two extra channels have been used (as "Dummy") in order to draw less current from the HV generators. The sketch is not to scale.

LAPPD signal with amplitude greater than 20 mV (discriminator module used), coming from a single pad for 10 sec was counted using an electronic scalar module. Figure 1.6 illustrates the horizontal and vertical rate scans for pad #6 and the estimated coarse position is ∼(14 mm, 56 mm). The rate scans of other pads are not shown in this report.

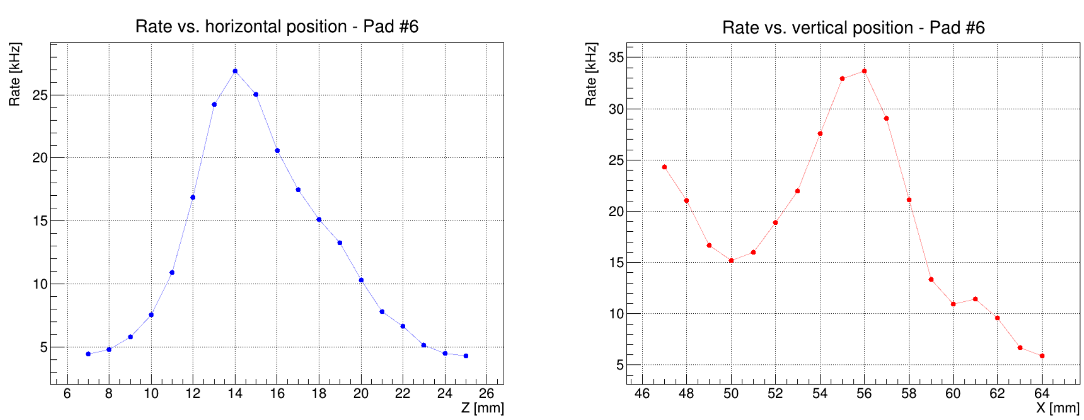

Figure 1.6: Horizontal (left) and vertical (right) rate scans, in a step of 1 mm, determine the coarse position ∼(z = 14 mm, x = 56 mm) of the sensor pad #6.

1.3 Measurements before substantial illumination

Two quantities of interest for the ageing studies were the QE and the signal amplitude. These quantities, as a function of horizontal coordinate of the sensor pad, had been measured for the eight pads. The QE is a measure of the number of coincidence events as a percentage of total of trigger events, whereas the signal amplitude is a measure of the integrated charge on the pad. The pulsed laser with an intensity of 1.7 and an external trigger rate (using a waveform generator) of $\sim$ 600 Hz was used for these measurements. Using CAEN V1742 digitizer module a 100k events had been registered for each measurement. During the data taking for a particular pad, other channels had been disconnected from the readout electronics. The efficiency scans for pads #1-2-4-3 and pads #5-6-8-7 are shown in clockwise direction from the top-left in Figures 1.7 and 1.8, respectively. The signal amplitude scans for pads #1-2-4-3 and pads #5-6-8-7 are shown in clockwise direction from the top-left in Figures 1.9 and 1.10, respectively. Position of the pads, as indicated by the vertical dotted lines, are vividly visible in these plots. Most of the QE values for the reference pads were around 5 % representing the Single Photo-Electron (SPE) production, whereas for the pads chosen to be exposed to substantial light integrals, the QE values were mostly greater than 10 %.

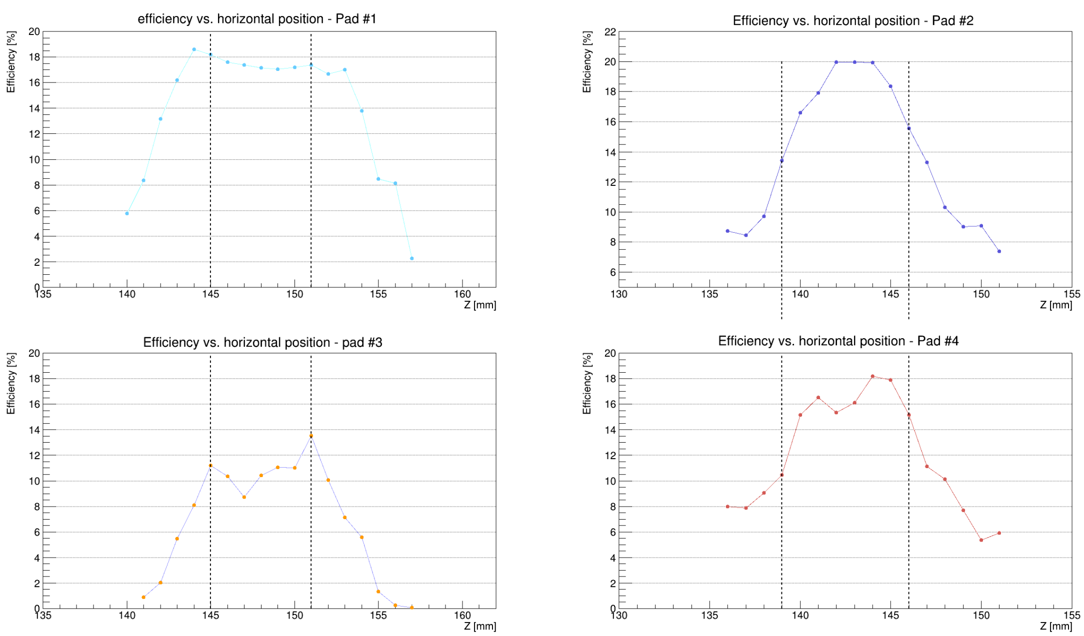

Figure 1.7: Quantum efficiency scans as a function of horizontal coordinate of the sensor pad #1 (top-left), #2 (top-right), #3 (bottom-left) and #4 (bottom-right) are measured. The vertical dotted lines show the position of the pad.

1.4 Integrated charge at the photocathode

A region of area $\sim 4.53\ cm^2$ on the LAPPD window that was aligned with sensor pads #1-2-3-4 was illuminated by substantial light from a continuous LED. The illumination happened in two steps: 3 hours followed by 10 hours on the following day. The

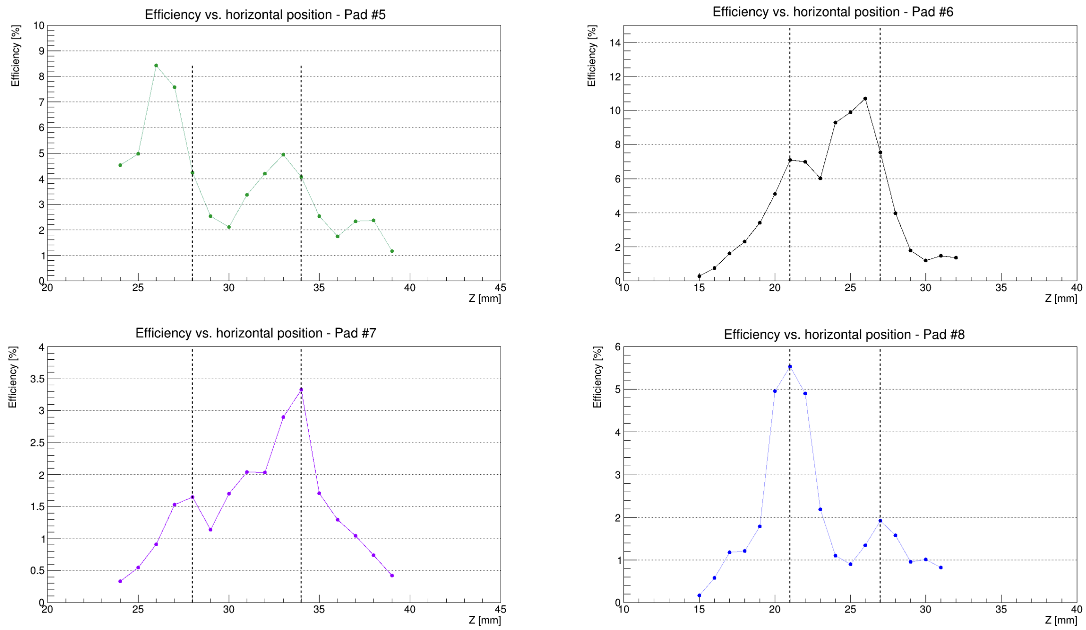

Figure 1.8: Quantum efficiency scans as a function of horizontal coordinate of the sensor pad #5 (top-left), #6 (top-right), #7 (bottom-left) and #8 (bottom-right) are measured. The vertical dotted lines show the position of the pad.

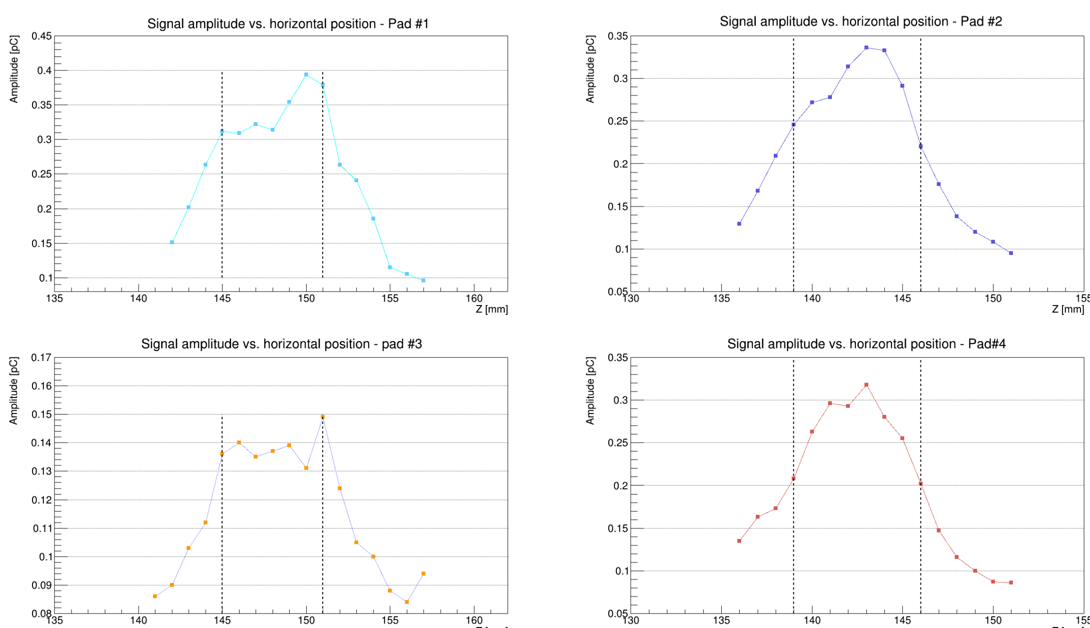

Figure 1.9: Signal amplitude scans as a function of horizontal coordinate of the sensor pad #1 (top-left), #2 (top-right), #3 (bottom-left) and #4 (bottom-right) are measured. The vertical dotted lines show the position of the pad.

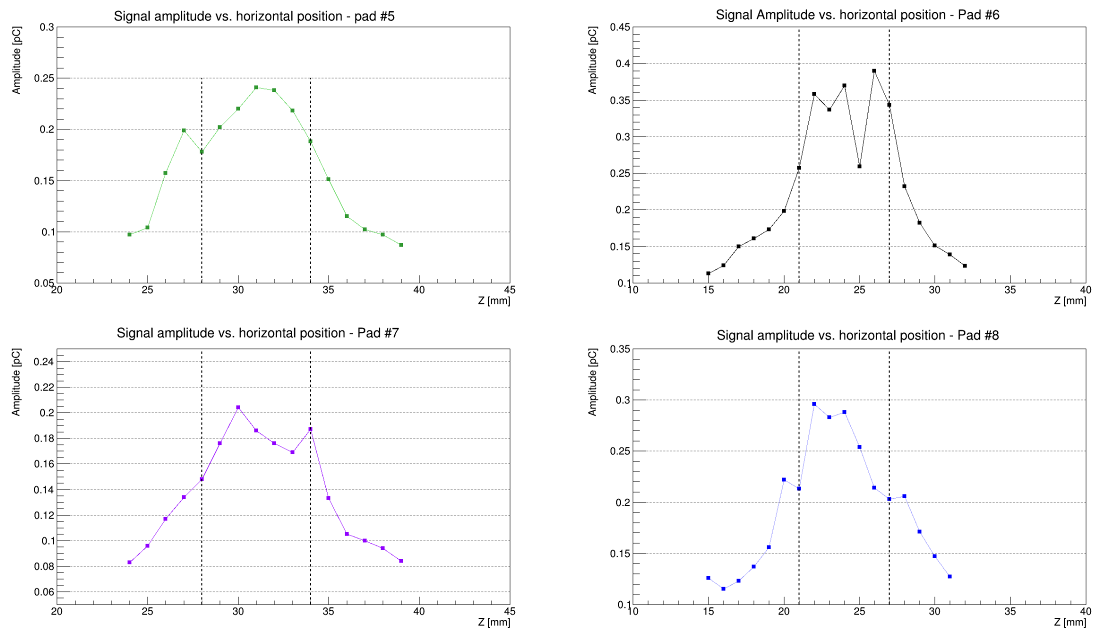

Figure 1.10: Signal amplitude scans as a function of horizontal coordinate of the sensor pad #5 (top-left), #6 (top-right), #7 (bottom-left) and #8 (bottom-right) are measured. The vertical dotted lines show the position of the pad.

set current, measured current and measured voltage (i.e., the forward bias voltage) of the LED were 16 mA, 15 mA and 2.90 V, respectively. The corresponding PC current measured by a custom-designed picoammeter had been visualised online (Figure 1.11) and stored using vplot software program running on a Linux computer. The program stored two values of current per second (hence, X-axis title is time [0.5 sec]). Figure 1.12 shows the jump, decay pattern and drop in the PC current as a function of time, when the continuous LED was turned ON, illuminating the region for 3 hours and turned OFF, respectively. A ~ 50 % drop in the PC current was observed during the 3 hours of illumination. The readings of PC current, indeed, were negative and were multiplied by (-1) in the code that was used for data analysing.

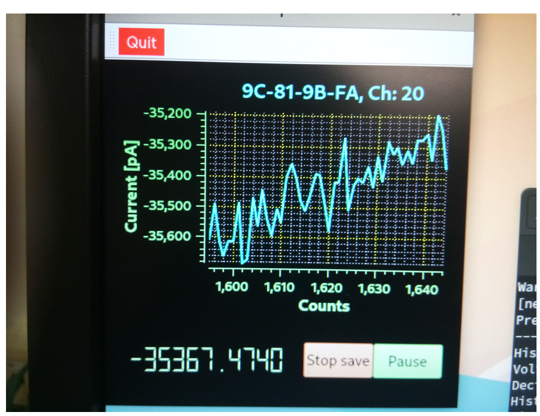

Figure 1.11: Online visualisation of the PC current as a function of time is managed by vplot software program.

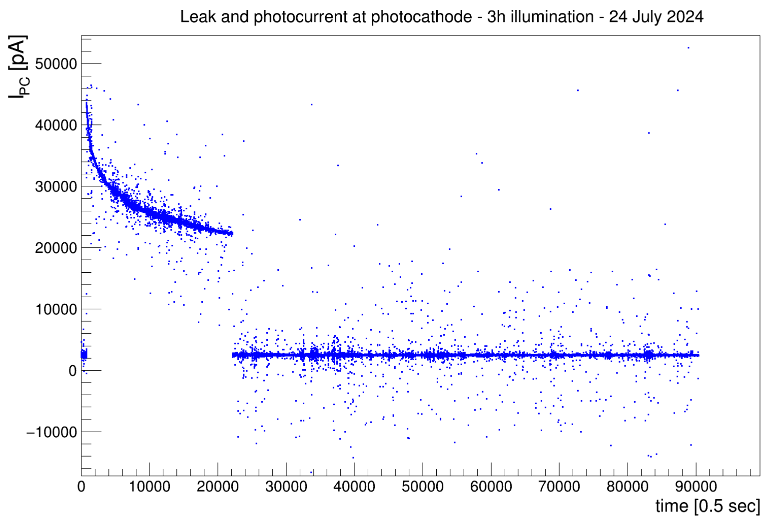

Figure 1.12: The current at the Photocathode before, during and after exposing $\sim$ 4.53 cm^2 area of the LAPPD window to substantial illumination, as a function of time, has been measured. A decay pattern with a $\sim$ 50 % drop in the PC current has been observed during the 3 hours of illumination.

In order to make an estimation of the photocurrent at the PC it is required to make an estimation of the average PC current before and after the substantial illumination happened. In this text we refer this component as the leak current. Figures 1.13-left and 1.13-right show the two distributions of leak current, fitted with Gaussian functions, at the PC before and after 3 hours of illumination, respectively. Mean values of these distributions were extracted from the fitting parameters: the values were 2.57 $\pm$ 0.05 nA and 2.50 $\pm$ 0.05 nA. So, the estimated average PC leak current was:

$$\begin{aligned} I_L^{PC} &= \frac{(2.57 + 2.50)}{2}\, nA \\ &= 2.54\, nA \end{aligned} \tag{1.1}$$

On the other hand, Figure 1.14-right shows the distribution of total PC current during the illumination of light. The mean value of the distribution was 26.36 nA. Hence, the average estimated photocurrent at the PC during the 3 hours of illumination was:

$$\begin{aligned} I_{3h}^{PC} &= I_{L+3h}^{PC} - I_L^{PC} \\ &= (26.36 - 2.54)\, nA \\ &= 23.82\, nA \end{aligned} \tag{1.2}$$

Hence, the estimated global integrated charge at the PC after the 3 hours of exposure was:

$$\begin{aligned} Q_{3h}^{PC} &= \int I_{3h}^{PC} dt \\ &= 23.82\, nA \;\times 10800\, s \\ &\approx 0.257\, mC \end{aligned} \tag{1.3}$$

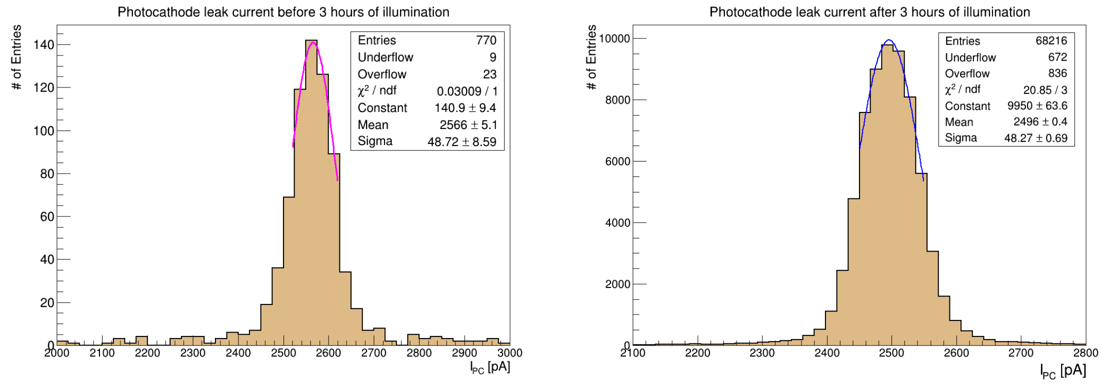

Figure 1.13: Distributions of Photocathode leak current before (left) and after (right) the 3 hours of illumination are fitted with Gaussian functions and the average values extracted from the fitting parameters are 2.57 ± 0.05 nA and 2.50 ± 0.05 nA, respectively.

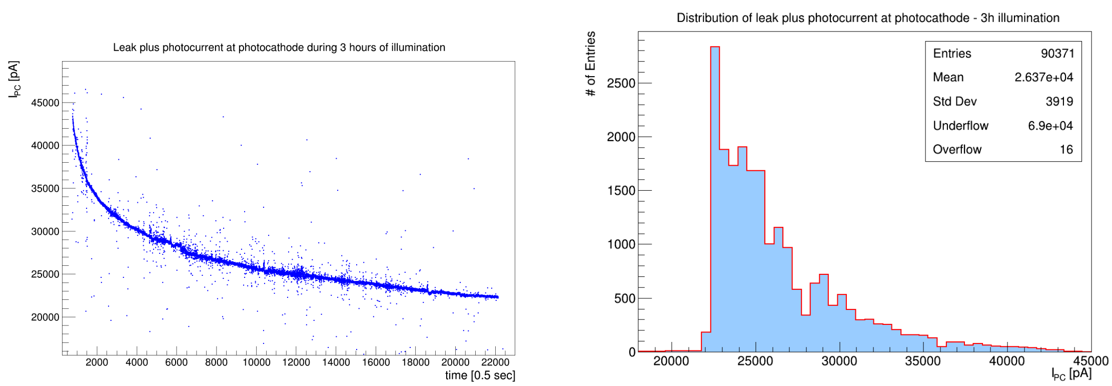

Figure 1.14: Total current at the Photocathode during the 3 hours of illumination: its evolution in time (left) and its distribution with a mean value of 26.36 nA (right).

In a second step, the mentioned region of the LAPPD window was exposed to substantial light for 10 hours. For the stability of the detector the distance between the window and fibre tip was increased further by 1-2 cm. Figure 1.15 shows the evolution of the PC current in time. A ∼ 46 % drop in the current was observed during the illumination. Figures 1.16-left and 1.16-right show two distributions of leak current at the PC and the estimated average PC leak current before and after the 10 hours of illumination was obtained in a similar fashion as before:

$$\begin{aligned} I_L^{PC} &= \frac{2.45 + 2.59}{2} nA \\ &= 2.52\, nA. \end{aligned} \tag{1.4}$$

Figure 1.17-right shows the distribution of total PC current with an average value of 16.29 nA during the 10 hours of exposure. Hence, the average estimated global photocurrent at the PC during the second step of illumination was:

$$\begin{aligned} I_{10h}^{PC} &= I_{L+10h}^{PC} - I_L^{PC} \\ &= 13.77\, nA \end{aligned} \tag{1.5}$$

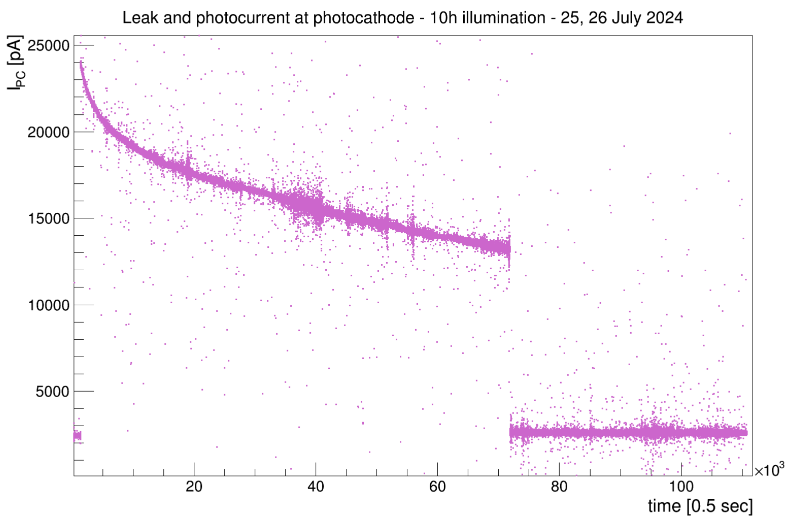

Figure 1.15: The current at the Photocathode before, during and after exposing $\sim 4.53\ cm^2$ area of the LAPPD window to substantial illumination, as a function of time, has been measured. A decay pattern with a ~ 46 % drop in the PC current has been observed during the 10 hours of illumination.

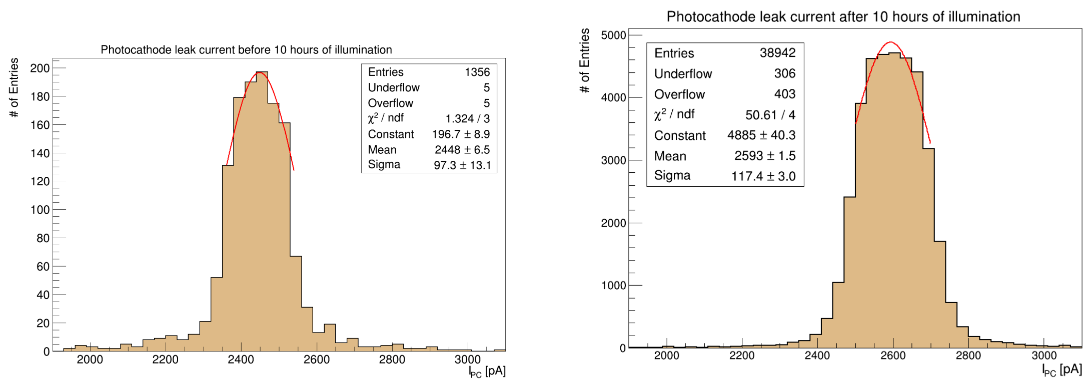

Figure 1.16: Distributions of Photocathode leak current before (left) and after (right) the 10 hours of illumination are fitted with Gaussian functions and the average values extracted from the fitting parameters are 2.45 ± 0.10 nA and 2.59 ± 0.12 nA, respectively.

This provided the estimated global integrated charge at the PC after the 10 hours of illumination:

$$
\begin{aligned}
Q^{PC}_{10h} &= \int I^{PC}_{10h}\, dt \\
&= 13.77\, nA\ \times 36000\, s \\
&\approx 0.496\, mC
\end{aligned}
\tag{1.6}
$$

Hence, the total global integrated ‘photon related charge’ at the PC after 13 hours of

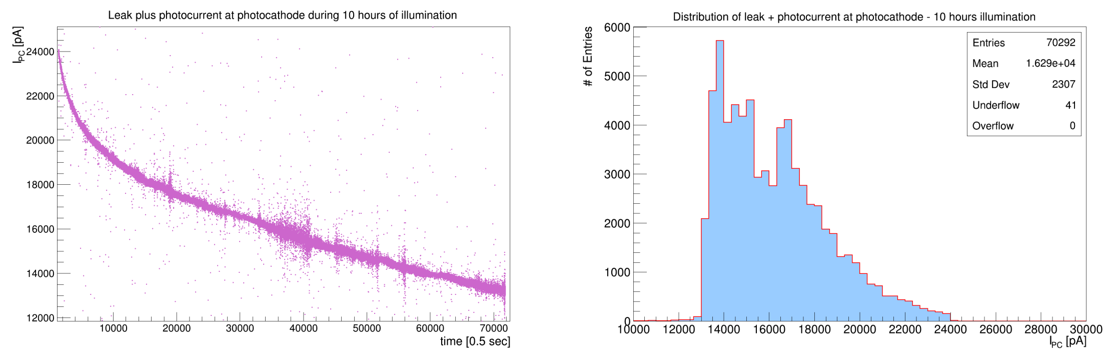

Figure 1.17: Total current at the Photocathode during the 10 hours of illumination: its evolution in time (left) and its distribution with a mean value of 16.29 nA (right).

substantial illumination was:

$$\begin{aligned} Q_{13h}^{PC} &= (0.257 + 0.496)\, mC \\ &= 0.753\, mC \\ N_{PE} &= \frac{0.753\, mC}{1.6 \times 10^{-19}\, C} \\ &\approx 47 \times 10^{14} \end{aligned} \tag{1.7}$$

where N_{PE} is the number of photoelectrons. The charge Q_{13h}^{PC} was spread almost uniformly on the surface of area 4.53 cm^2.

1.4.1 Signal amplitude suppression

It was observed that during substantial illumination on the selected area of the window, LAPPD signal (with amplitude > 20 mV) rates individually on pads # 1-2-3-4 were almost zero. This fact can be described as the suppression of signal amplitude due to high illumination. It seemed that the LAPPD was not able to process the accumulated (space) charge that eventually reduced the electric field and led to this "zero-gain" state of the detector. The signal rates for individual pads during substantial illumination are listed in Table 1.1. It was clearly visible that the reference pads #5-6-7-8 were receiving a small fraction of the illumination that made the signal rates on these pads more than a factor twice of their DCRs (see next Section 1.5).

Pad #	1	2	3	4	5	6	7	8
Signal rates [kHz]	0.0	0.0	0.0	0.0	12.6	12.9	12.9	14.2

Table 1.1: Signal rates on individual pads measured at some point during the exposure of the small area of the LAPPD window to substantial illumination, are listed.

1.5 Effects of ageing

After exposing a small region of the LAPPD window to substantial illumination for 13 hours, measurements of QEs and signal amplitudes were repeated. In this report we will show the ageing effects after illumination only for pads #1 and #4 (highly illuminated ones) and pads #6 and #7 (reference pads). In Figure 1.18-left QE as a function of horizontal coordinate of the pad #1 measured before illumination, after 3 hours of illumination and after 13 hours of illumination has been shown, where an overall 60 % drop in the values, after the 13 hours of illumination, can be observed. Similarly, in Figure 1.18-right more that 65 % drop in the QE can be observed for the pad #4. On the other hand, for the reference pads #6 and #7, as shown in Figures 1.19-left and 1.19-right, the QE remained unchanged within 2 % after the 13 hours of illumination. Comparing these two cases we could affirm that the significant drop in the QE for pads #1 and #4 was a clear evidence of ageing.

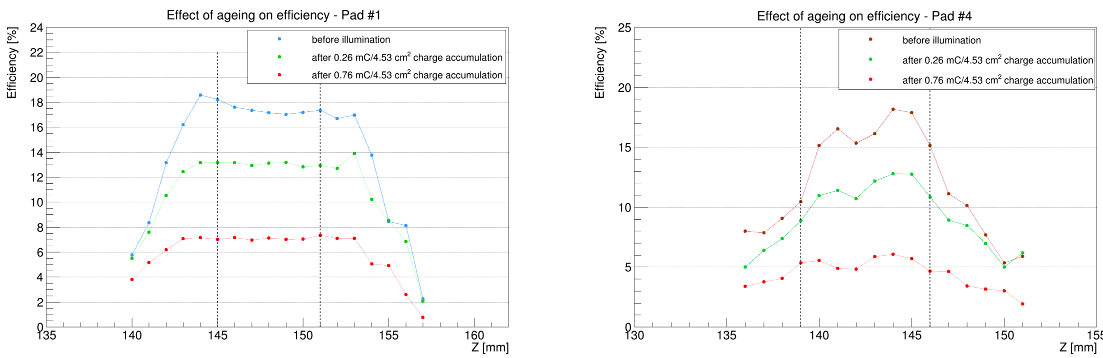

Figure 1.18: Quantum Efficiency as a function of horizontal coordinate of the pad #1 (left) and pad #4 (right) has been measured before illumination, after 3 hours of illumination and after 13 hours of illumination. Significant drop in the efficiency, that provides a clear indication of ageing, has been observed.

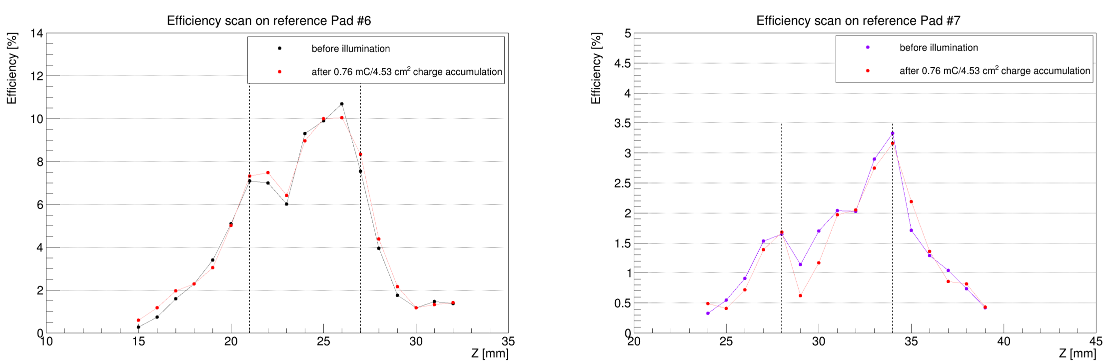

Figure 1.19: Quantum Efficiency as a function of horizontal coordinate of the pad #6 (left) and pad #7 (right) has been measured before illumination, after 3 hours of illumination and after 13 hours of illumination. No evidence of ageing is present in the data.

On the contrary, the effect of ageing on signal amplitude was neither evident nor clear. The signal amplitudes for pads #1 and #4 increased by ∼10 % after 13 hours of illumination as shown in Figures 1.20-left and 1.20-right, whereas the signal amplitudes for pads #6 and #7 remained unchanged within ∼5 %, though for some points modification was upto ∼ 25 % as can be seen in Figures 1.21-left and 1.21-right.

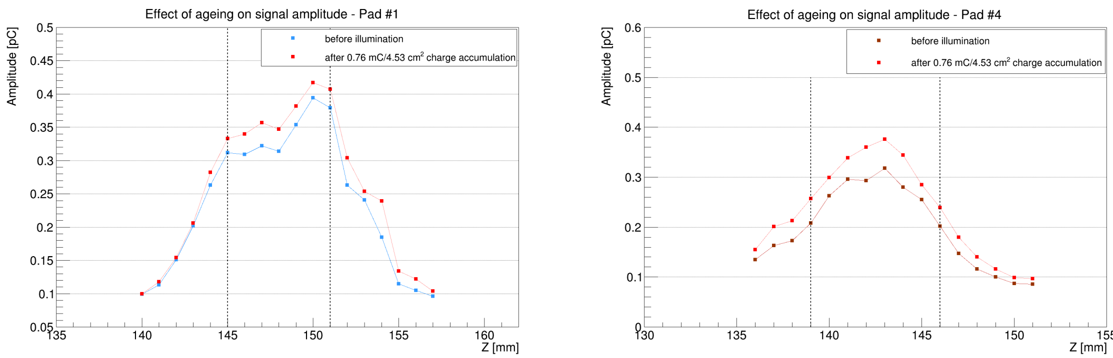

Figure 1.20: Signal amplitude as a function of horizontal coordinate of the pad #1 (left) and pad #4 (right) has been measured before illumination, and after 13 hours of illumination. There is a 10 % rise in the amplitude.

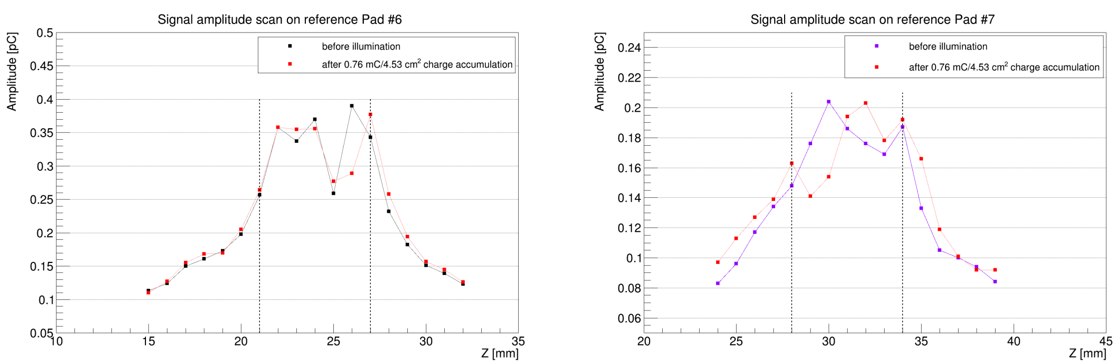

Figure 1.21: Signal amplitude as a function of horizontal coordinate of the pad #6 (left) and pad #7 (right) has been measured before illumination and after 13 hours of illumination. The values are consistent within 5 % apart from few points that show significant modification.

Another important quantity to observe ageing effects on the PC was the DCR. DCRs for all eight pads were measured on three consecutive days before exposing the LAPPD window to substantial illumination. Observed values were consistent within a factor $\sim$ 1.5. While for the reference pads the DCRs were less than 6 kHz, for the pads chosen for substantial illumination they were greater than 15 kHz, apart from the values for the pad #3 that showed much smaller values of a few hundred Hz. After 13 hours of exposure measurements were repeated. For pads #1-2-3-4 that received substantial illumination, the DCRs reduced by a factor 3 or more, leaving a clear evidence of ageing, while for the reference pads the DCRs remained similar within a factor $\sim$ 1.5. All the relevant numbers are listed in Table 1.2.

1.6 Integrated charge at the Anode

In this section we will evaluate the amount of integrated charge, after 13 hours of illumination, at the Anode. Due to some technical and software related problems we were not able to store the readings from the Keithley in a datafile. A good alternative

Dark Count Rates [kHz] (Threshold > 20 mV)				
Pad #	Before illumination Day1	Day2	Day3	After illumination [0.76 mC/4.53 cm^2]
1	16.0	16.6	18.8	6.65
2	23.0	27.3	42.8	7.93
3	0.2	0.2	0.3	3.94
4	16.2	16.8	23.7	6.38
5	5.4	6.3	5.5	4.00
6	4.1	5.2	3.8	3.42
7	5.2	3.4	4.0	4.85
8	2.2	3.3	2.8	2.41

Table 1.2: Dark Count Rates measured before and after exposing 4.53 cm^2 area of the LAPPD window to substantial illumination, are listed. The reduction in numbers for pads #1-2-3-4 show a clear evidence of ageing.

was to make a correlation between the Keithley current (written down in the logbook as a function of time) and the CAEN HV current (monitored by geco2020 software) at XoX and eventually, extract the mean Anode current during the illumination from the distribution of XoX current. Figures 1.22-left and 1.22-right show the evolution of currents before, during and after the 3 hours of illumination at the XoX and NoX, respectively. It can be seen that the current at the NoX went above 800 μA leading to a lack of voltage stability of this electrode. For a couple of times during the measurement the monitoring software displayed 'ovp' as the HV status of the electrode, followed by a stepping down in the HV and finally turning Off the HV channel. (It was NOT the case when the monitored current reached the CAEN limit.)

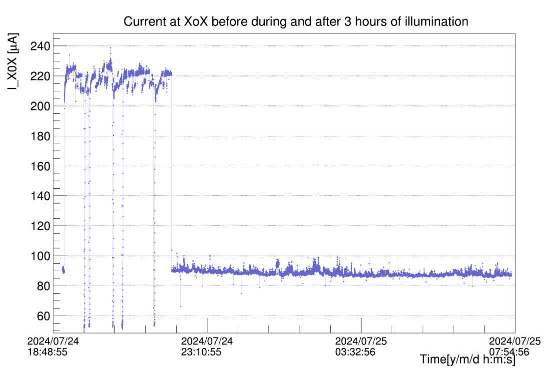

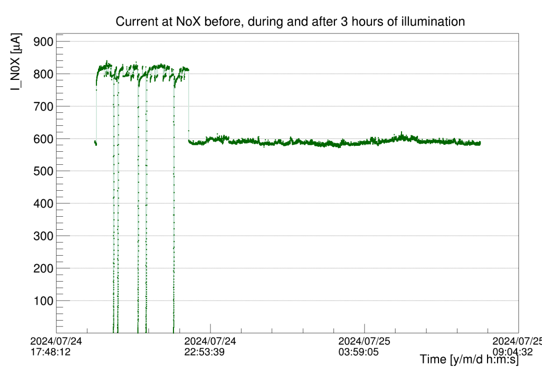

Figure 1.22: The evolution of CAEN monitored currents before, during and after 3 hours of illumination at the Exit of Exit and Entry of Exit electrodes are shown.

In order to make an estimation of the 'photon related current' at the XoX it is required to make an estimation of the average XoX current before and after the substantial illumination happened. As before we refer to this component as the leak current. Figures 1.23-left and 1.23-right show the two distributions of leak current at the XoX before and after 3 hours of illumination, respectively. The distribution on the left was fitted with a Gaussian function and the mean was extracted from the fitting parameter.

The correlation between the Anode leak current and the XoX leak current was:

$$I_L^A = I_L^{XoX} + 66.67\,\mu A \tag{1.8}$$

where 66 .67 μA traversed through the 3 MΩ resistor shown in the circuit of Figure 1.5. So, the anode leak currents before and after the illumination were: (90.26 – 66.67) μA = 23.59 μA and (88.25 – 66.67) μA = 21.58 μA, respectively. So, the estimated constant anode leak current was:

$$\begin{aligned} I_L^A &= \frac{(23.59 + 21.58)}{2}\,\mu A \\ &\approx 22.59\,nA \end{aligned} \tag{1.9}$$

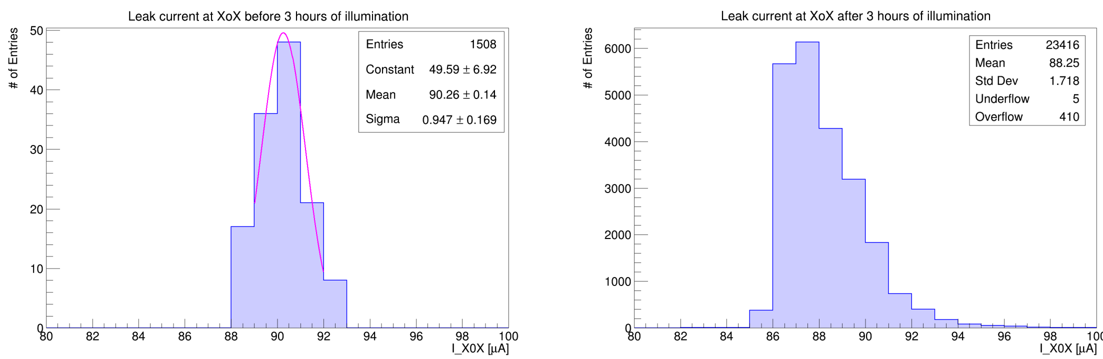

Figure 1.23: Distributions of XoX leak current before (left) and after (right) the 3 hours of illumination are shown. The mean values of these distributions are 90.26 μA (from the Gaussian fit) and 88.25 μA, respectively.

The correlation between the Anode current and the XoX current was modified during illumination of substantial light. The similar trends of these currents and a scatter plot depicting their correlation are shown in Figures 1.24-left and 1.24-right, respectively. The correlation equation extracted from the linear fit was:

$$I_{3h}^A = I_{3h}^{XoX} + 54.0\,\mu A \tag{1.10}$$

On the other hand, the distribution of total XoX current during the 3 hours of illumination is shown in Figure 1.25. The mean of this distribution was $\sim$ 219 μA. So, the mean total current at the anode was (219 - 54) μA = 165 μA. Hence, the light induced anodic current during the 3 hours was:

$$\begin{aligned} I_{3h}^A &= I_{L+3h}^A - I_L^A \\ &= (165.0 - 22.59)\,\mu A \\ &= 142.41\,\mu A \end{aligned} \tag{1.11}$$

Hence, the estimated global integrated charge at the Anode after the 3 hours was:

$$\begin{aligned} Q_{3h}^A &= \int I_{3h}^A dt \\ &= 142.41\,\mu A \, \times 10800\,s \\ &\approx 1.538\,C \end{aligned} \tag{1.12}$$

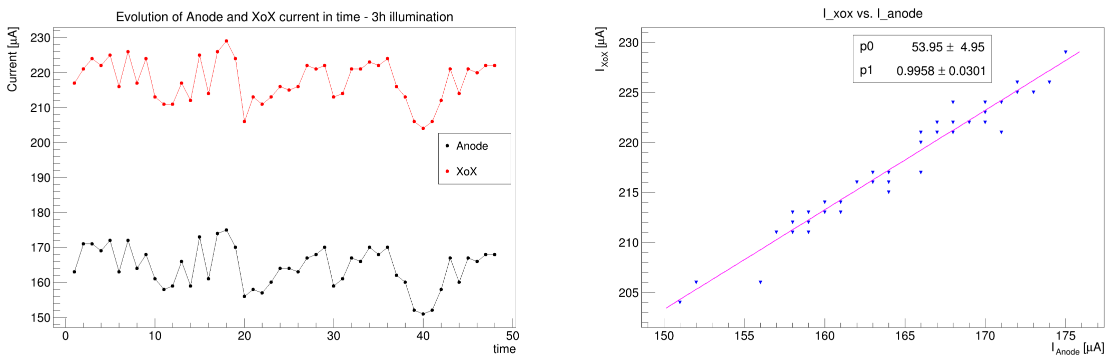

Figure 1.24: Evolution of currents at the Anode and XoX in time (left) and the corresponding scatter plot fitted with a linear function (right), during the 3 hours of illumination.

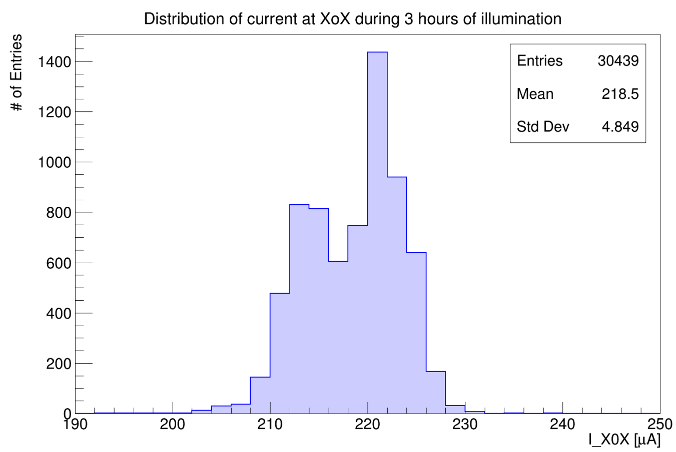

Figure 1.25: The distribution of total current at the XoX during the 3 hours of illumination.

In the second step of illumination for 10 hours the distance between the LAPPD window and the fibre tip from the continuous LED was increased by 1-2 cm. As a result, the currents at the XoX and NoX were stable as can be seen in Figures 1.26-left and 1.26-right. The average leak current before and after the 10 hours at the XoX was obtained in a similar manner as mentioned above. The corresponding distributions are shown in Figures 1.27-left and 1.27-right. So, the anode leak currents before and after the illumination were: $(84.95 - 66.67)\ \mu\text{A} = 18.28\ \mu\text{A}$ and $(90.56 - 66.67)\ \mu\text{A} = 23.89\ \mu\text{A}$, respectively. So, the estimated constant anode leak current was:

$$\begin{aligned} I_L^A &= \frac{(18.28 + 23.89)}{2}\,\mu A \\ &\approx 21.00\,\mu A \end{aligned} \tag{1.13}$$

The correlation between the Anode current and XoX current during the 10 hours was similar to Equation 1.10. The evolution of these currents in time and a scatter plot depicting their correlation are shown in Figures 1.28-left and 1.28-right, respectively.

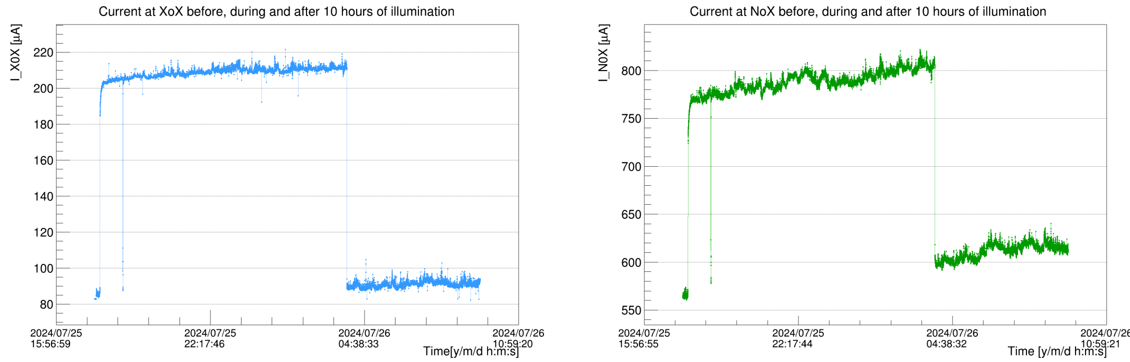

Figure 1.26: The evolution of CAEN monitored currents before, during and after 10 hours of illumination at the Exit of Exit and Entry of Exit electrodes are shown.

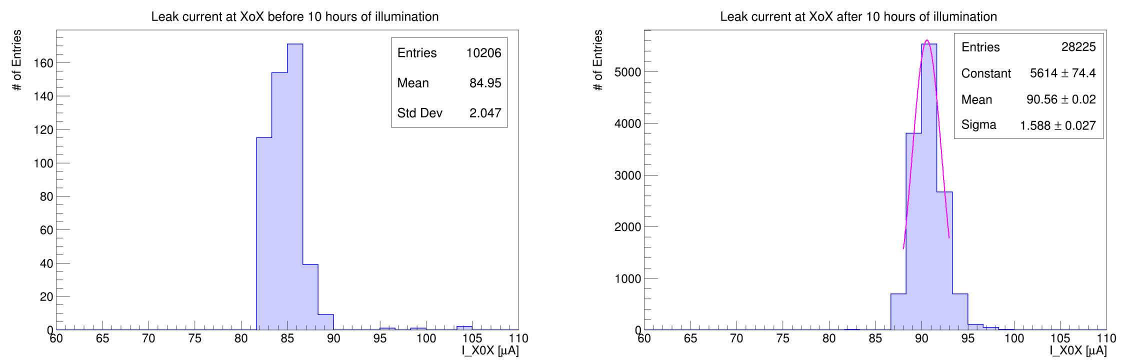

Figure 1.27: Distributions of XoX leak current before (left) and after (right) the 10 hours of illumination are shown. The mean values of these distributions are 84.95 μA and 90.56 μA (from the Gaussian fit), respectively.

The linear fit provided:

$$I_{10h}^{A} = I_{10h}^{XoX} + 55.0\,\mu A \tag{1.14}$$

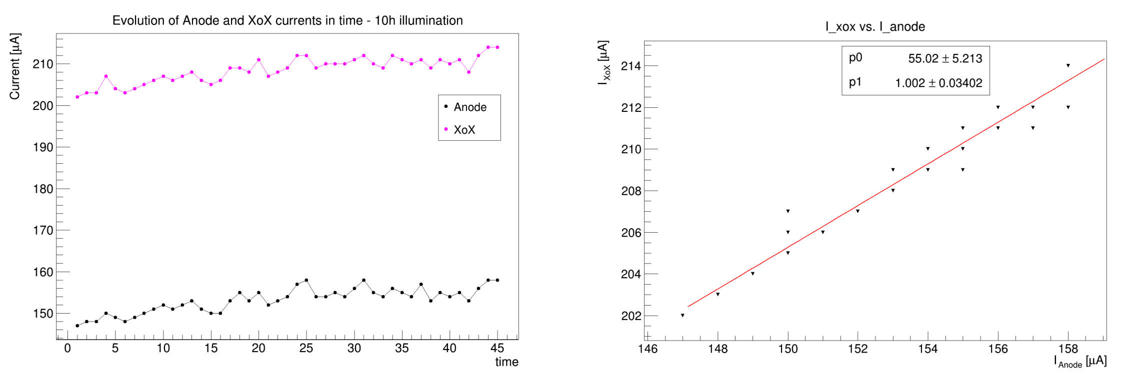

Figure 1.28: Evolution of currents at the Anode and XoX in time (left) and the corresponding scatter plot fitted with a linear function (right), during the 10 hours of illumination.

The distribution of total XoX current during the 10 hours of illumination is shown in Figure 1.29. The mean of this distribution was $\sim 209\ \mu$A. So, the total current at the anode was (209 - 55) μA = 154 μA. Hence, the light induced anodic current during the 10 hours was:

$$\begin{aligned} I^A_{10h} &= I^A_{L+10h} - I^A_L \\ &= (154.0 - 21.00)\,\mu A \\ &= 133.0\,\mu A \end{aligned} \tag{1.15}$$

So, the estimated global integrated charge at the Anode after the 10 hours was:

$$\begin{aligned} Q^A_{10h} &= \int I^A_{10h} dt \\ &= 133.0\,\mu A\ \times 36000\,s \\ &\approx 4.788\,C \end{aligned} \tag{1.16}$$

Hence, the total global integrated "photon related charge" at the Anode after 13 hours of substantial illumination was:

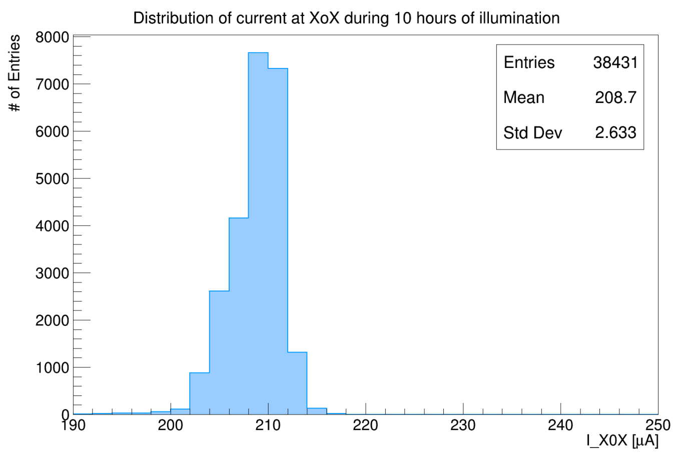

Figure 1.29: The distribution of total current at the XoX during the 10 hours of illumination.

$$\begin{aligned} Q^A_{13h} &= (1.538 + 4.788)\,C \\ &= 6.326\,C \end{aligned} \tag{1.17}$$

The ratio of the total integrated charge at the Anode and that at the PC was:

$$\begin{aligned} R^Q_{13h} &= \frac{6326}{0.753} \\ &\approx 8401 \end{aligned} \tag{1.18}$$

1.7 Output-input current ratio at MCPs

In this section we will look at the evolution and distribution of the XoN current (CAEN values) during substantial illumination. Figure 1.30 shows the evolution of XoN current before, during and after the 3 hours of illumination. The distribution of the corresponding leak and total current are shown in Figures 1.31-left and 1.31-right. The "photon-related current" was extracted by subtracting the mean values of the distributions: (258.8 - 246.1) μA= 12.7 μA. Similarly, the same can be obtained for the 10 hours of illumination. The Plots are shown in Figure 1.32 and Figures 1.33-left and 1.33-right. The "photon-related current" was found to be: (256.6 - 246.2) μA= 10.4 μA.

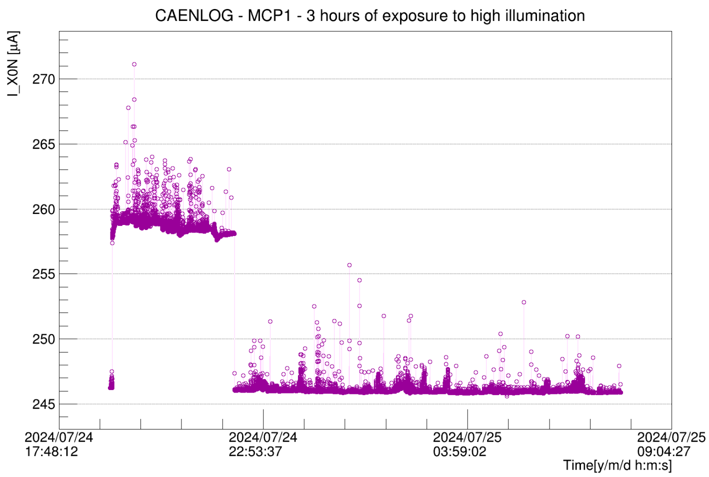

Figure 1.30: The evolution of current at the XoN during the 3 hours of illumination.

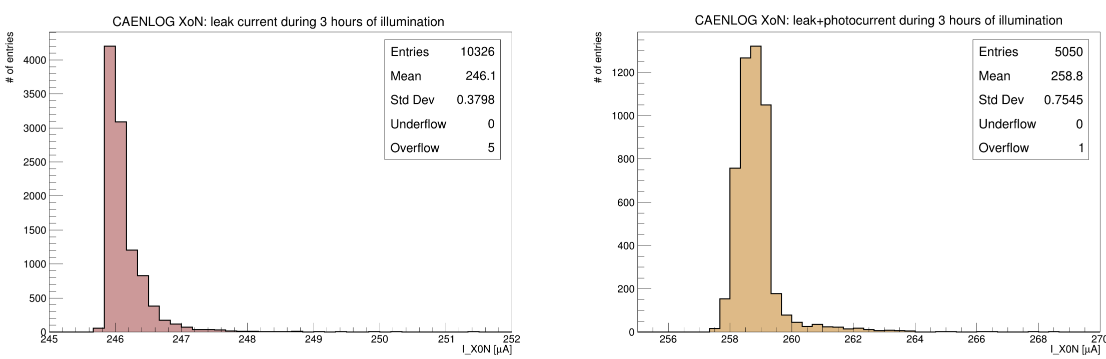

Figure 1.31: Distribution of the leak (left) and total (right) current at the XoN during the 3 hours of illumination.

From the "photon-related current" at the PC (Section 1.4), XoN and Anode (Section 1.6) we can estimate the LAPPD gain during the illumination at the individual MCP level. Here gain is expressed as the ratio of the output and input current, i.e., the ratio of I_{XoN} and I_{PC} for the Entry MCP and the ratio of I_A and I_{XoN} for the Exit MCP. All the relevant numbers along with the effective gain of the LAPPD are listed in Table 1.3.

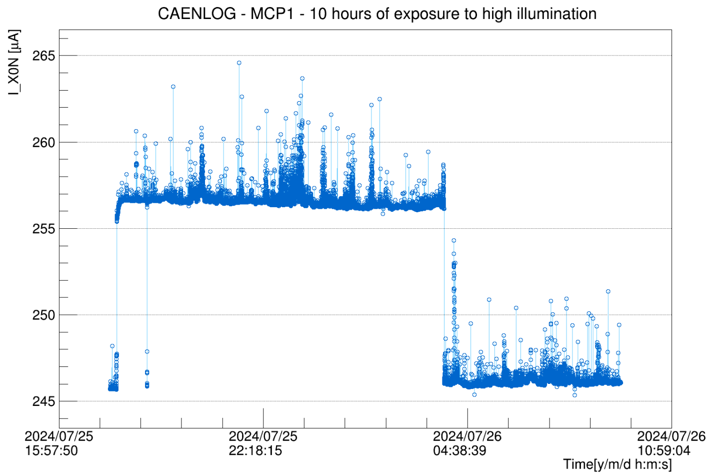

Figure 1.32: The evolution of current at the XoN during the 10 hours of illumination.

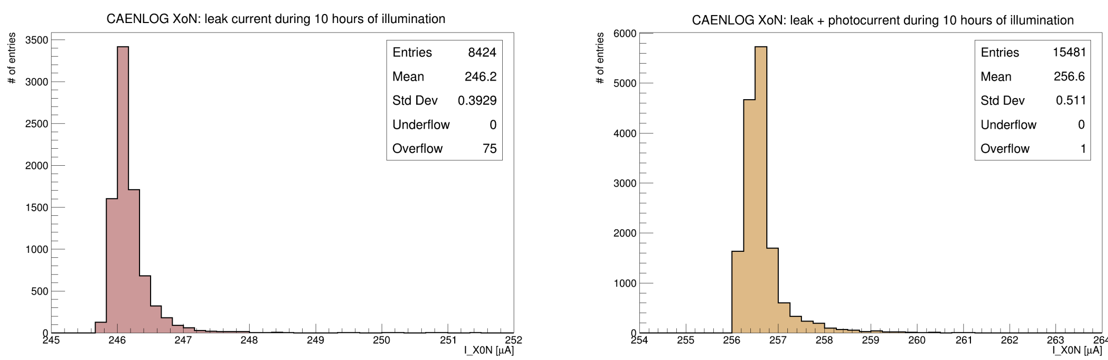

Figure 1.33: Distribution of the leak (left) and total (right) current at the XoN during the 10 hours of illumination.

Duration [h]	Photon-related current @			Current ratio		Gain
(continuous light)	PC [nA]	XoN [μA]	Anode [μA]	G1 = $\frac{I_{NoX}}{I_{PC}}$	G2 = $\frac{I_{Anode}}{I_{XoN}}$	G1 $\times$ G2
3	23.8	12.7	141.7	534	11	5874 $\sim 6 \times 10^3$
10	13.8	10.4	132.2	754	13	9802 $\sim 10^4$

Table 1.3: The ratio of output and input current individually after the two MCP layers, during the ageing tests for the 3 and 10 hours of substantial illumination, are listed. The corresponding effective gains have also been calculated.

Studies with pulsed LED

Some tests with the pulsed laser source were performed before the ageing studies. For these tests a different custom-designed PCB with central pads connected was used. The repetition frequency of the internal trigger for the pulsed laser was set at 80 MHz/32 (2.5 MHz) and the three intensities that had been used were 2.8, 3.3 and 3.8. So, the amount of light was definitely higher than that required for SPE production. The reason for these higher intensities is to have sufficient light to be able to measure the photocurrent from the leak current, in particular, at the PC. The biasing configuration of the LAPPD for these tests, was the same as mentioned in the ageing studies, i.e., the differential HV potential applied at XoX-NoX-XoN-NoN-PC were 200-825-200-825-30 V, respectively. The " photon-related current" values at the XoX and Anode were same for the pulsed light. The correlation was $I_{X0X} = I_A + 66.67\ \mu$A. For the " photon-related current" values at XoX or Anode both the CAEN current at XoX (as a function of time) and the Keithley current (the average value by eye estimation) were recorder.

The goal of these measurements, initially, was to check if ageing can be performed using pulsed light at higher repetition frequency for couple of days. It was observed that it will take months to do so. Later the measurements were used to compare the ratio of output and input currents at the two MCP levels as function of intensities. For each intensity, measurements of currents were taken for $\sim$ 10 min-10 min-10 min-10 min ($\sim$ 40 min in total) keeping the laser On-Off-On-Off, respectively.

In the following section the evolution of currents at the PC, X0N and XoX (Anode) in time and their corresponding distributions, for the above mentioned intensities are shown. The photon related current has been extracted by subtracting the leak from the total current.

2.1 Output-input current ratio at MCPs

2.1.1 Intensity 3.8

The current vs. time plots for the NoN, XoN, XoX and NoX, when the pulsed laser was in states On-Off-On-Off, ten minutes at each state and with an intensity of 3.8 for the 'On' states, are shown respectively from the top-left in clockwise direction in Figures 2.1. Applying cuts on the time axis the photon related currents at the XoN and XoX were extracted. Individually, for the second On state and the two Off states, the

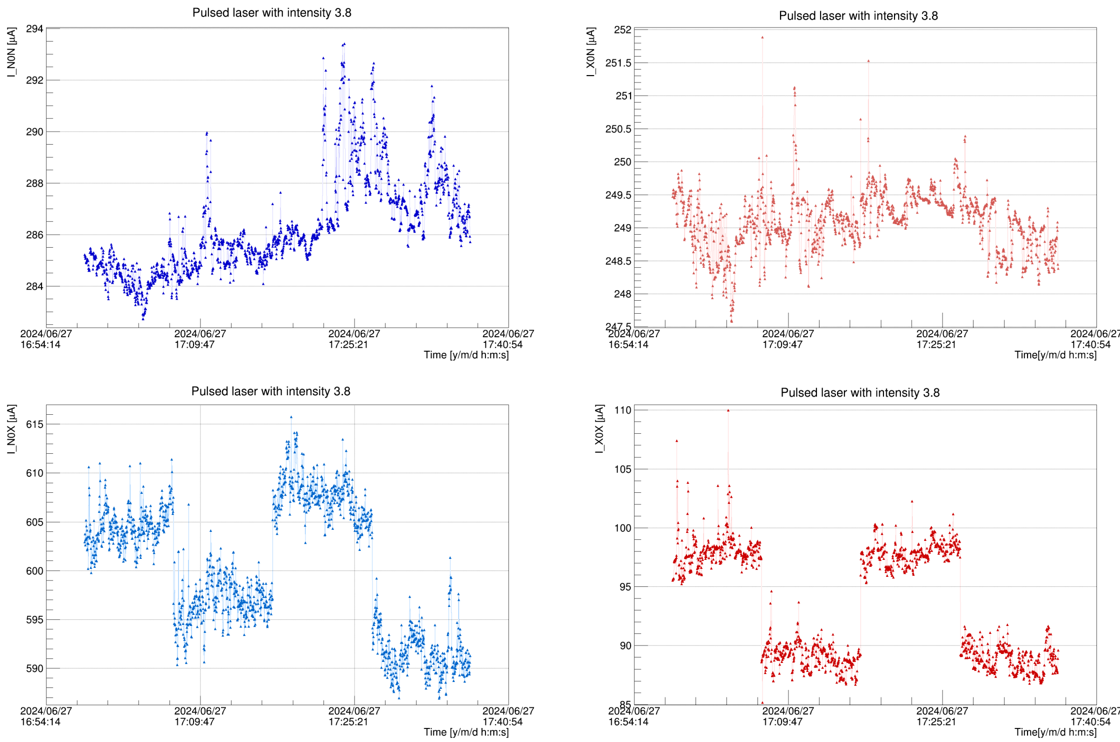

Figure 2.1: The evolution of CAEN currents at the NoN (top-left), XoN (top-right), NoX (bottom-left) and XoX (bottom-right) electrodes as a function of time, when the pulsed laser intensity was set at 3.8, are shown.

mean of the distributions of the XoN current were 249.4 μA and 249.0 μA, as shown in Figures 2.2-left and 2.2-right, respectively, and it provided the "photon related current" as 0.4 μA. Similarly, for same cuts the mean of the distributions of the XoX current were 97.8 μA and 88.8 μA as shown in Figures 2.3-left and 2.3-right, respectively. So, the "photon related current" at the XoX/Anode was 9 μA. Also the Keithley provided the same value: (35-26) μA = 9 μA.

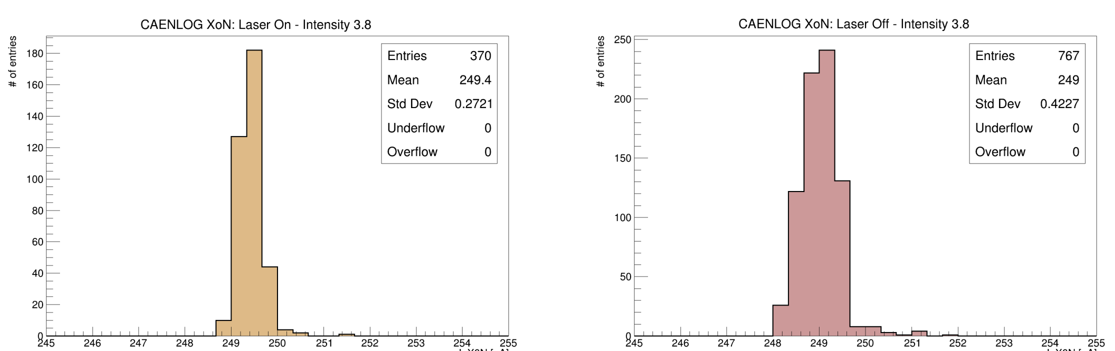

Figure 2.2: The distribution of XoN current for the two OFF states (left) and the second On state (right) are displayed. The difference of the two mean values is the estimation of the "photon related current" that is 0.4 μA.

The evolution of corresponding PC current in time and its distribution are shown

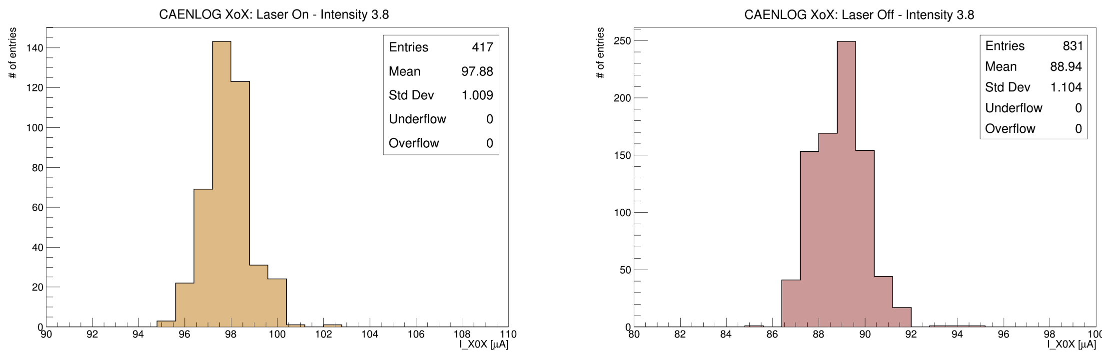

Figure 2.3: The distribution of XoX current for the two OFF states (left) and the second On state (right)are displayed. The difference of the two mean values is the estimation of the "photon related current" that is 9.0 μA.

in Figures 2.4-left and 2.4-right, respectively. The two peaks are well resolved and subtracting the mean values of the peaks, i.e., the leak from total current, we can estimate the PC photocurrent at laser intensity 3.8:

$$
\begin{aligned}
I^{PC}_{\gamma,3.8} &= I^{PC}_{Tot} - I^{PC}_{L} \\
&= (2894 - 2724)\, pA \\
&= 170\, pA
\end{aligned} \tag{2.1}
$$

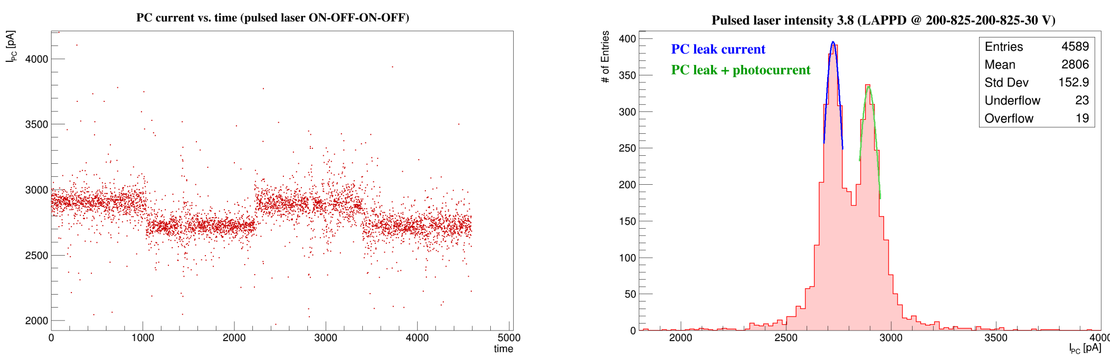

Figure 2.4: The evolution of the Photocathode current in time (left) and its distribution (right), when the laser intensity was set at 3.8, are shown.

The ratio of the output and input currents at both MCP levels, for the laser intensity set at 3.8, are listed in Table 2.1. Similar ratios were extracted when the laser intensity was set at 3.3 and 2.8. These numbers are also put together in the table. All relevant plots for intensities 3.3 and 2.8 are illustrated in the next Sections 2.1.2 and 2.1.3. The signal rates (amplitude $>$ 20 mV) measured using an oscilloscope, and hence, the photon detection efficiency, for the three intensities, are also noted down in Table 2.1. For making a comparison, similar values from the ageing studies (Table 1.3) are inserted below this table.

There was no linear correlation between the "photon-related current" at the Anode and that at the PC for the three intensities as shown in Figure 2.5-left. Similar exercise was performed, historically before the above mentioned tests, at a different biasing

Intensity (pulsed light)	Signal rate (>20 mV) [kHz]	Photon-related current @			Current ratio		Gain
		PC [pA]	XoN [μA]	XoX [μA]	G1 = $\frac{I_{NoX}}{I_{PC}}$	G2 = $\frac{I_{XoX}}{I_{XoN}}$	G1 × G2
3.8	1100 (44 %)	170	0.4	9.0	2353	23	$\sim 5.4 \times 10^4$
3.3	700 (28 %)	70	0.3	6.0	4286	20	$\sim 8.6 \times 10^4$
2.8	450 (18 %)	16	0.1	5.0	6250	50	$\sim 3.1 \times 10^5$
Duration [h] (continuous light)	-	Photon-related current @			Current ratio		Gain
	-	PC [nA]	XoN [μA]	Anode [μA]	G1 = $\frac{I_{NoX}}{I_{PC}}$	G2 = $\frac{I_{Anode}}{I_{XoN}}$	G1 × G2
3	-	23.8	12.7	141.7	534	11	$5874 \sim 6 \times 10^3$
10	-	13.8	10.4	132.2	754	13	$9802 \sim 10^4$

Table 2.1: The ratio of output and input current individually after the two MCP layers, for the laser intensity set at 3.8, 3.3 and 2.8, are listed. The corresponding effective gains have also been calculated. Using the signal rates and the given repetition frequency of 2.5 MHz the effective efficiency for each of the cases has been measured. For comparison the similar values obtained during the ageing studies, that are listed in Table 1.3, are inserted in the last two rows.

configuration of the LAPPD, i.e., 200-875-200-875-50 V, with the same repetition frequency of the laser and from intensity 2.2 to 4.9. It can be observed in Figure 2.5-right that up-to intensity 3.3, there is a linearity with a gain of $\sim 3 \times 10^5$, but for higher intensities the gain decreased by a factor of 3.

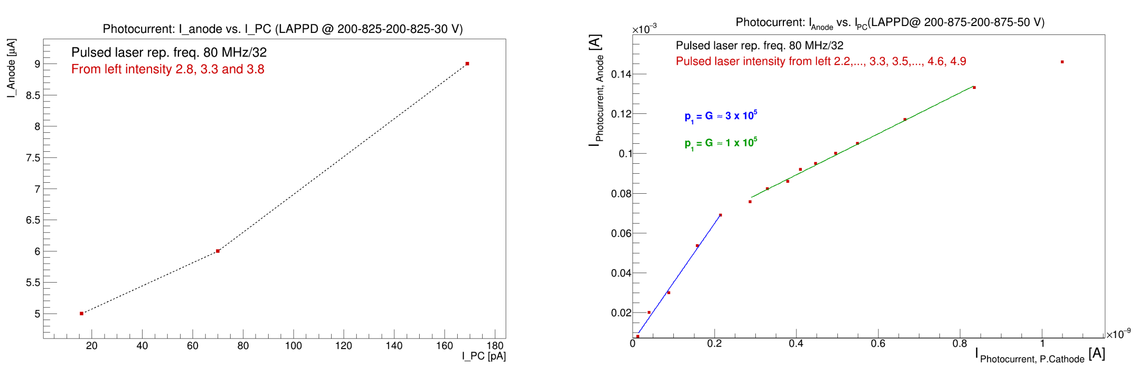

Figure 2.5: The correlation between the "photon-related current" at the Anode and that at the Photocathode for different intensities of the pulsed laser are, when the LAPPD is kept at 200-825-200-825-30 V (left) and 200-875-200-875-50 V (right), are shown. Linearity has been observed in the latter and the slope decreases for higher intensities of light.

2.1.2 Intensity 3.3

Current vs time plots and some of their distributions for the laser intensity set at 3.3 are shown in Figures 2.6, 2.7 and 2.8.

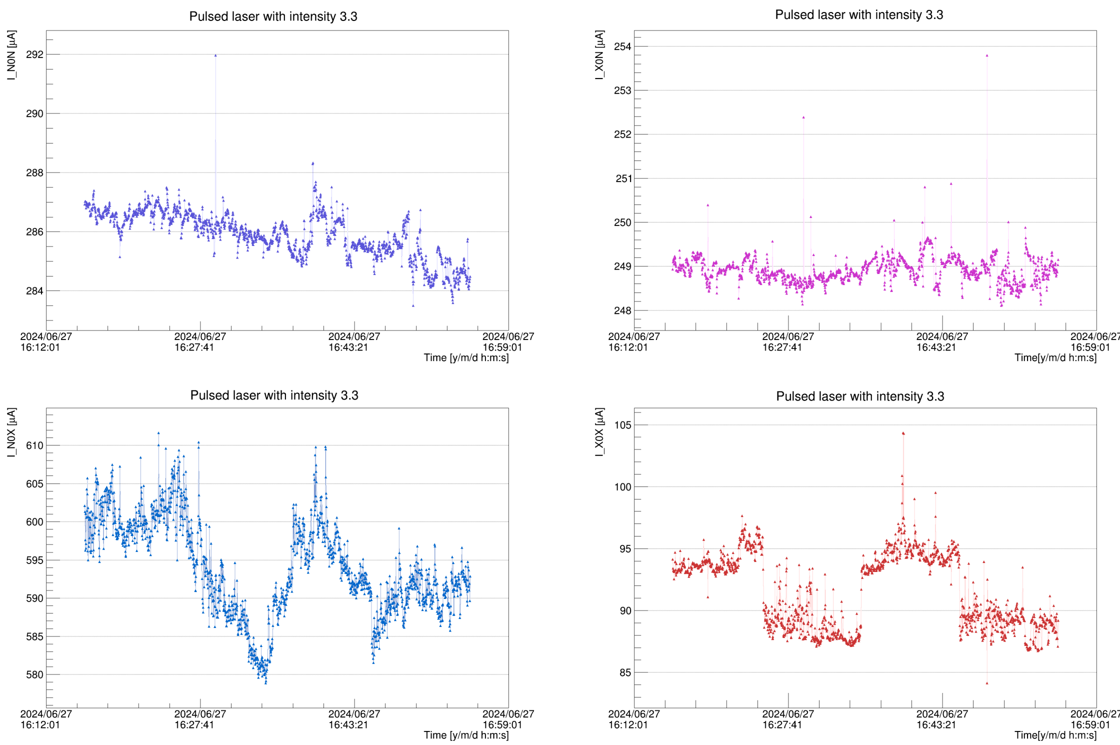

Figure 2.6: The evolution of CAEN currents at the NoN (top-left), XoN (top-right), NoX (bottom-left) and XoX (bottom-right) electrodes as a function of time, when the pulsed laser intensity was set at 3.3, are shown.

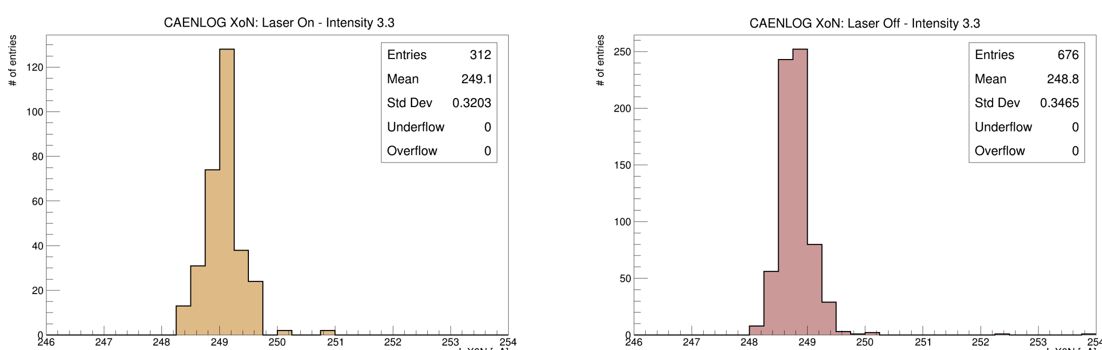

Figure 2.7: The distribution of XoN current for the two OFF states (left) and the second On state (right) are displayed. The difference of the two mean values is the estimation of the “photon related current” that is 0.3 μA.

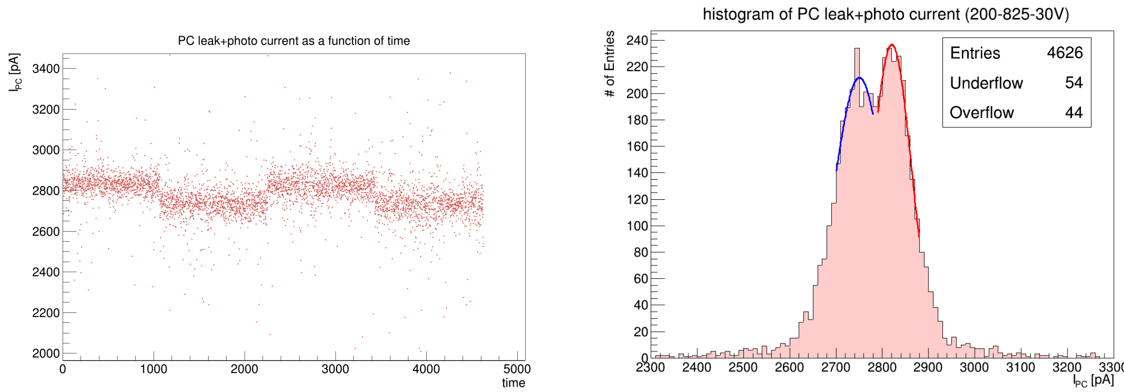

Figure 2.8: The evolution of the Photocathode current in time (left) and its distribution (right), when the laser intensity was set at 3.3, are shown.

2.1.3 Intensity 2.8

Current vs time plots and some of their distributions for the laser intensity set at 3.3 are shown in Figures 2.9, 2.10, 2.11 and 2.12.

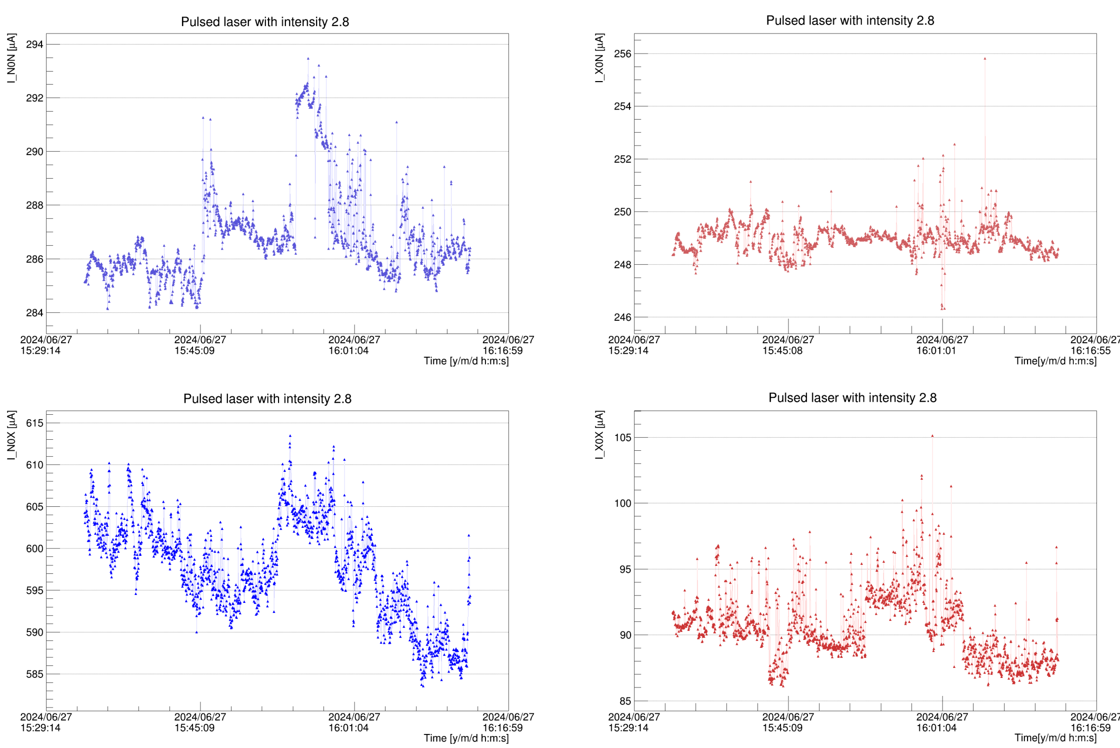

Figure 2.9: The evolution of CAEN currents at the NoN (top-left), XoN (top-right), NoX (bottom-left) and XoX (bottom-right) electrodes as a function of time, when the pulsed laser intensity was set at 2.8, are shown.

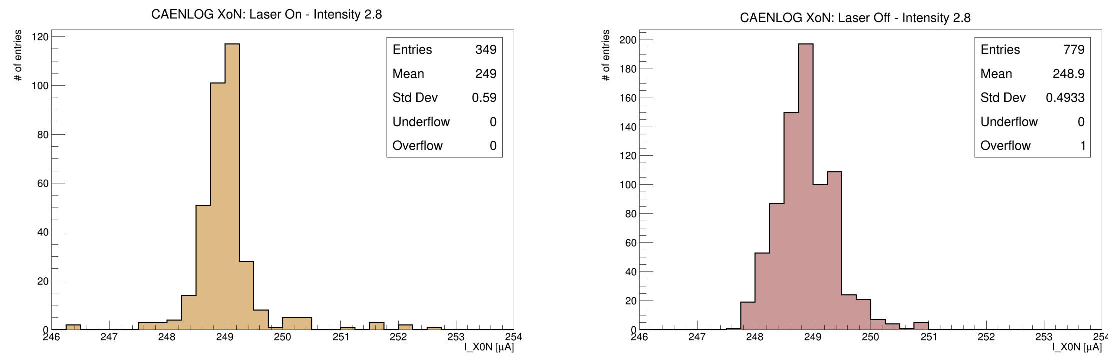

Figure 2.10: The distribution of XoN current for the two OFF states (left) and the second On state (right) are displayed. The difference of the two mean values is the estimation of the "photon related current" that is 0.1 μA.

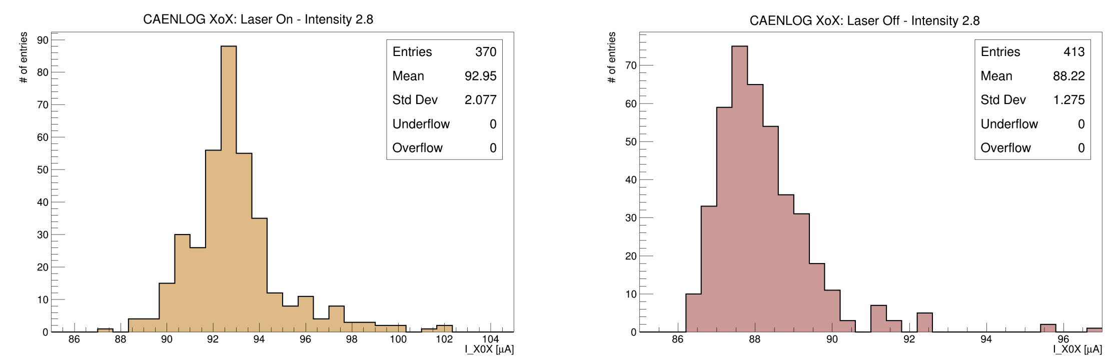

Figure 2.11: The distribution of XoX current for the two OFF states (left) and the second On state (right) are displayed. The difference of the two mean values is the estimation of the "photon related current" that is 5.0 μA.

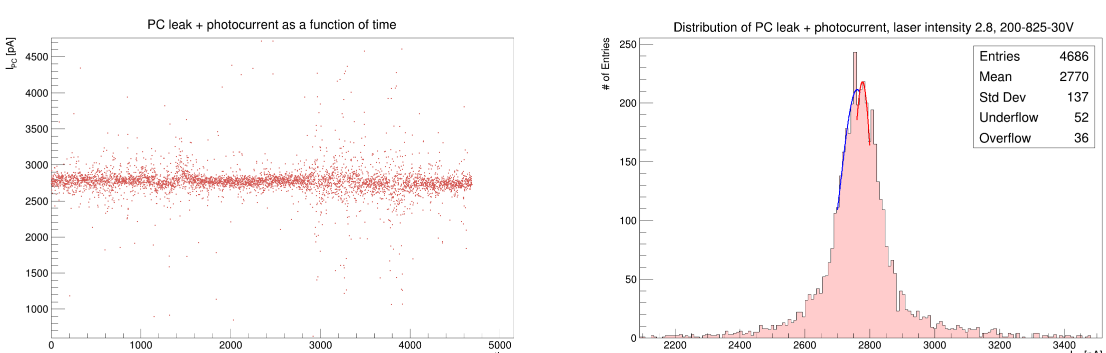

Figure 2.12: The evolution of the Photocathode current in time (left) and its distribution (right), when the laser intensity was set at 2.8, are shown.

CAEN current distribution

Here we will show the presence of parasitic resistances (or leaks) in the electronic circuit as understood from the CAEN and Keithley current values of the Exit MCP and Anode, respectively. CAEN currents had few tens of nA offsets for better resolution, whereas the offset increased by a factor 10 for worse resolution. In Figure 3.1 the electrical circuit has been sketched for a particular voltage configuration of the LAPPD. The PC and Entry MCP are not shown as they are kept at zero differential potential. The Anode leak current (measured by the Keithley) as a function of voltage at the XoX had been measured as shown in Figure 3.2. The Ohmic resistance extracted from the fitting parameter of the linear function was $\sim$ 19 GΩ. On the other hand, $R^{'}$ in the circuit can be derived using the following equation:

$$\begin{aligned} \frac{\Delta V_{XoX}}{I_{XoX}} &= R_L^{XoX} \\ &= \left[\frac{1}{R_L^A} + \frac{1}{R^{'}}\right]^{-1} \end{aligned} \tag{3.1}$$

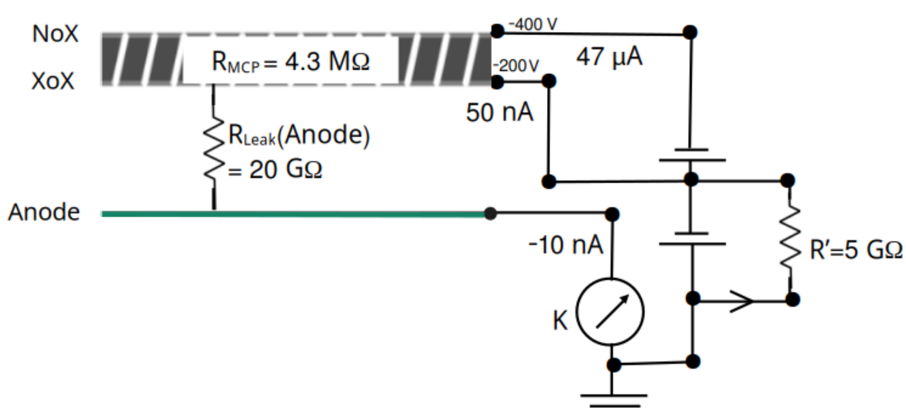

Figure 3.1: The presence of parasitic resistances for a particular biasing configuration of the Exit MCP is sketched with all values of voltages, currents and resistances. The other electrodes of the LAPPD are kept at -400 V i.e., zero differential potential are applied. Unlike R_L^A, $R^{'}$ shows non-Ohmic behaviour.

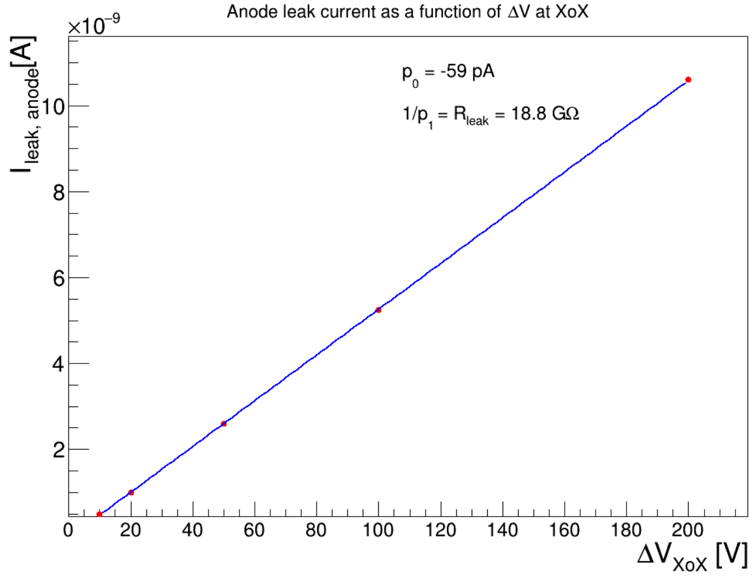

Figure 3.2: The anode leak current as a function of ΔV_{XoX}, has been measured. It shows an Ohmic behaviour and the slope extracted from the linear fit function is $\sim$ 19 GΩ.

We measured the values of $R^{'}$ and also the resistance of the Exit MCP for different voltage configuration of the Exit MCP. All relevant values are listed in Table 3.1. Case-I was measured keeping the 3 MΩ resistor between the XoX and the ground, whereas case-II was the similar configuration, but without the 3 MΩ resistor.

Case	ΔV_{XoX} $= V_{XoX}$ [V]	ΔV_{NoX} [V]	V_{NoX} [V]	I_{XoX} [nA]	I_{NoX} [μA]	I_K [nA]	$R_L^A = \frac{\Delta V_{XoX}}{I_K}$ [GΩ]	$R^{'}$ $\sim$f(R_L^{XoX}) [GΩ]	$R^{MCP} = \frac{\Delta V_{NoX}}{I_{NoX}}$ [MΩ]
I	- 200	0	- 200	66800	-	- 10	20	-	-
II	- 100	0	- 100	10	-	- 5	20	20	-
III	- 200	- 200	- 400	50	47	-10	20	5	4.3
IV	- 100	- 100	- 200	16	22	- 5	20	9	4.5
V	- 200	- 100	- 300	36	22	- 10	20	7.7	4.5
VI	- 200	- 300	- 500	63	77	- 12.2	20	4	3.9
VII	- 200	- 500	- 700	125	153	- 40	20	1.7	3.3
VIII	- 200	- 400	- 600	85	111	- 20	20	2.7	-
IX	- 200	- 800	- 1000	1300	354	- 1000	?	0.15	2.3
X	- 200	- 875	- 1075	2900	438	- 2500	?	0.07	-

Table 3.1: CAEN currents at the XoX and NoX as well as the keithley current at the Anode, for different biasing configuration of the XoX and NoX, are listed. Corresponding values of R_L^A, $R^{'}$ and R^{MCP} are also listed. All other electrodes of the LAPPD were kept at the same potential as that of the NoX by applying zero differential HV potentials.